Bioactive Materials 6 (2021) 4506–4516

Contents lists available at ScienceDirect

Bioactive Materials

journal homepage: www.sciencedirect.com/journal/bioactive-materials

Capturing dynamic biological signals *via* bio-mimicking hydrogel for precise remodeling of soft tissue

Zhengwei Cai [a,b,1], Qimanguli Saiding [c,1], Liang Cheng [a], Liucheng Zhang [a], Zhen Wang [a], Fei Wang [a], Xinliang Chen [c], Gang Chen [b], Lianfu Deng [a], Wenguo Cui [a,*]

[a] Department of Orthopaedics, Shanghai Key Laboratory for Prevention and Treatment of Bone and Joint Diseases, Shanghai Institute of Traumatology and Orthopaedics, Ruijin Hospital, Shanghai Jiao Tong University School of Medicine, 197 Ruijin 2nd Road, Shanghai, 200025, PR China

[b] Jiaxing Key Laboratory of Basic Research and Clinical Translation on Orthopedic Biomaterials, Department of Orthopaedics, The Second Affiliated Hospital of Jiaxing University, 1518 North Huancheng Road, Jiaxing, 314000, China

[c] Shanghai Key Laboratory of Embryo Original Diseases, The International Peace Maternal and Child Health Hospital, School of Medicine, Shanghai Jiao Tong University, 910 Hengshan Road, Shanghai, 200030, PR China

ARTICLE INFO

Keywords:
Biological signals
Physiological phase
Hydrogel
Chemotactic
Soft tissue remodeling

ABSTRACT

Soft tissue remodeling is a sophisticated process that sequentially provides dynamic biological signals to guide cell behavior. However, capturing these signals within hydrogel and directing over time has still been unrealized owing to the poor comprehension of physiological processes. Here, a bio-mimicking hydrogel is designed via thiol-ene click reaction to capture the early physical signal triggered by inflammation, and the chemical signals provided with chemokine and natural adhesion sites, which guaranteed the precise soft tissue remodeling. This bio-mimicking hydrogel efficiently facilitated cell anchoring, migration, and invasion in the 3D matrix due to the permissive space and the interaction with integrin receptors. Besides, the covalently grafted chemokine-like peptide is optimal for colonization and functional differentiation of endothelial cells through a HIF-1α dependent signal pathway. Furthermore, the early polarization of macrophages, collagen deposition and angiogenesis in rat acute wound model, and the increased blood perfusion in mouse skin flap model have confirmed that the bio-mimicking hydrogel realized precise soft tissue remodeling and opens new avenues for the phased repair of different tissues such as nerve, myocardium, and even bone.

1. Introduction

Soft tissue injuries caused by tumor resection, external trauma, natural aging, and congenital malformations bring tremendous mental pressure and economical loss to families and society. The physiological regeneration process of damaged soft tissue is quite complicated which includes dynamic physical and chemical signals over three phases: acute inflammatory phase (Phase I), basic immune response to endogenous and/or exogenous stimuli, and trigger matrix degradation to initiate the regeneration process; subacute repairing phase (Phase II), an intermediate stage during which the degradation of matrix together with releasing chemokines induce the migration and recruitment of neighboring cells; chronic reconstruction phase (Phase III), a terminal stage that provides natural adhesion sites for supporting the colonization and functional differentiation of regenerative cells [1–3]. Hydrogel is a polymer network that has mechanical properties and spatial structure similar to natural soft tissue [4–6]. Commercial hydrogel products have shown the ability to accelerate soft tissue repairs such as skin wounds, facial defects, and tendon injuries, but usually failing in capturing the related signals at different physiological phases to precisely adapt to the physiological regeneration process [7,8]. For instance, polyethylene glycol (PEG) hydrogels, despite their low immunogenicity, are nondegradable and lack the unique biochemical signals of natural extracellular matrix (ECM), thus lacking the responsiveness during the very early stage and inaptness for recruiting the regenerative cells during the later repairing phase [9,10]. Collagen and fibrin, abundant in natural tissues, owing to their quick degradation rate, the colonization and functional differentiation of cells during reconstruction is still unrealized [11,12].

Peer review under responsibility of KeAi Communications Co., Ltd.
* Corresponding author.
E-mail address: wgcui80@hotmail.com (W. Cui).
[1] These authors contributed equally to this work.

https://doi.org/10.1016/j.bioactmat.2021.04.039
Received 22 March 2021; Received in revised form 23 April 2021; Accepted 23 April 2021

Therefore, the ideal reconstructive hydrogel should be able to capture the variety of dynamic biological signals to fit the three physiological phases for precise soft tissue remodeling.

The acute inflammatory phase (Phase I) is the initiation of many physiological and pathological processes [13,14]. However, uncontrolled inflammation will continue to release excessive inflammatory mediators such as matrix metalloproteinases (MMPs), which will degrade the soft tissue and lead to persistent injury or scar formation [15]. MMP inhibitors have been used as anti-inflammatory approaches for soft tissue remodeling, however, many studies have shown that MMPs can degrade ECM and enhance chemokine activities during soft tissue repair indicative of the necessity of MMPs for tissue remodeling [16–18]. Given that, the hydrogel matrix should actively enable the inflammatory mediators to regulate the remodeling process. For example, Griffin et al. introduced MMP-sensitive peptides into hydrogel microspheres to provide sufficient space for immune cell infiltration and the subsequent migration of endothelial cells as well as other surrounding host cells [19]. Although the adaptation of the inflammatory phase is achieved in this way, it still lacks the dynamic biochemical signals for recruiting and communicating with host cells. Therefore, the hydrogel system needs to recapitulate more complex biological signals to induce the migration and morphogenesis of cells.

In Phase II, chemokines play a key regulatory role, not only participating in the process of early inflammatory cell recruitment but also inducing the migration of neighboring host cells to the injured site and promoting angiogenesis in tissue remodeling [20,21]. Therefore, it is an effective strategy to introduce chemokines into hydrogels to guide the recruitment and migration of host cells. Purcell et al. loaded recombinant stromal cell-derived factor-1 α (rSDF-1α) into hydrogel through electrostatic interaction and promoted the homing of

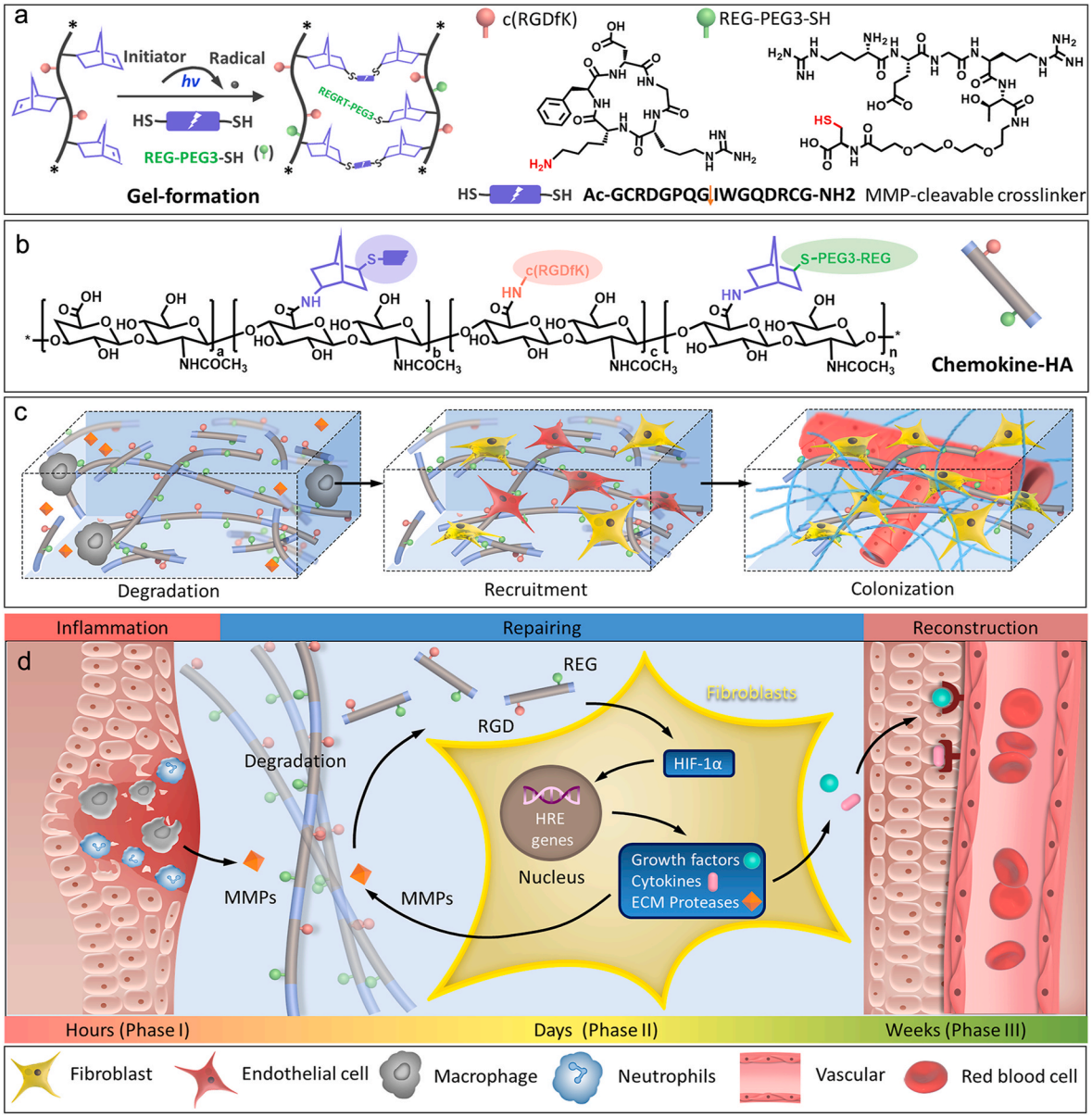

Fig. 1. Schematic illustrations of the hydrogel formation and matching the phases (I-III) of soft tissue regeneration. a) The degradation-recruitment-colonization integrated hydrogel were constructed by HA-NB-RGD, MMP-cleavable crosslinker, and chemokine-like peptide REG-PEG3-SH with thiol-ene click reaction. b) Enzymatic degradation and release of chemotactic hyaluronic acid fragments (chemokine-HA). c) Early inflammatory cells infiltrated hydrogel and released inflammatory mediators MMPs and the degraded hydrogel provided space for the recruitment, colonization, and functional differentiation of regenerative cells. d) Degradation, recruitment, and colonization of hydrogel were precisely matched with the inflammation of phase I, repairing of phase II, and reconstruction of phase III in soft tissue injury.

endogenous bone marrow-derived cells (BMCs) and myocardial tissue remodeling [22,23]. However, the enzymatic instability of chemokines and low loading efficiency limit its practicability to great extent. Small molecular peptides are another option to simulate chemokines due to their stable structure and high safety [24]. Recently, Wang et al. synthesized the short peptide REGRT, a cytokine derived from erythrocyte differentiation regulator 1 (Erdr1), and directly encapsulated it in hydrogel to promote wound healing [25]. However, the life span of bioactive peptides was too short for the physically encapsulated peptide to achieve a precise soft tissue remodeling, which strikes out the necessity of sufficient residence time to maintain the chemotactic activity of hydrogels during the wound healing process.

Natural ECM, composed of various proteins and polysaccharides, provides physical support and biological cues for cells during phase III [26,27]. The initial cell-matrix interaction is mediated through the binding of cell integrin and specific sequences of ECM (fibronectin: RGD; laminin: IKVAV, YIGSR, and collagen: GFOGER) [28]. Chaudhuri et al. covalently coupled RGD in alginate hydrogel to enhance cell adhesion and osteogenic differentiation *in vitro* [29]. Gjorevski et al. also design a polyethylene glycol (PEG) hydrogel grafted RGD to realize the survival and cloning of the intestinal crypts of mice and maintained their organ formation ability [30]. Although the introduction of adhesive peptides for the functional differentiation of cells and tissues *in vitro*, precise matching to the complex remodeling process of soft tissue injury *in vivo* still has not been achieved. Therefore, it is urgent to construct a bio-mimicking hydrogel with a phased response to soft tissue remodeling and functional feedback with the change of microenvironment.

Inspired by the physiological phases of soft tissue remodeling, we innovatively designed a bio-mimicking hydrogel via thiol-ene click reaction to capture the sequentially dynamic biological signals: degradation-recruitment-colonization to precisely fit the inflammation-repairing-reconstruction process of soft tissue remodeling (Fig. 1). Phase I: a MMPs cleavable hyaluronic acid (HA) hydrogel was obtained to achieve early inflammation-triggered matrix degradation and create sufficient space for the migration of neighboring host cells. Phase II: the chemokine-like peptide grafted onto HA (chemokine-HA) was released to form a dynamic communication between matrix degradation and cellular migration. Phase III: the RGD modified biomimetic HA hydrogel facilitated the colonization and functional differentiation of endothelial cells. The enzymatic degradation characteristics of the hydrogel matrix, the chemotactic activity of degradation products, and the colonization, as well as functional regulative capability on regenerative cells, were verified *in vitro*. Also, the reconstructive function of hydrogel on different soft tissue healing processes was further investigated by the rat acute wound model and mouse skin flap model *in vivo*.

2. Materials and method

2.1. Synthesis of hydrogels

All chemical reagents were purchased from commercial sources such as Sigma-Aldrich and Aladdin. Hyaluronic acid was purchased from Fruida (Shandong, China). c(RGDfK) (Mw = 603.6), Thiol modified REG REG-PEG3-SH (Mw = 924.0), and Matrix metalloproteinase substrate peptide Ac-GCRDGPQGIWGQDRCG-NH2 (Mw = 1745.8) were purchased from Apeptide (Shanghai, China). Unless specifically mentioned, the buffer used in the experiments is 0.01 M PBS (pH = 7.2).

Norbornene-functionalized HA (HA-NB) was prepared by the addition of norbornene amino via the 4-(4,6-Dimethoxy-1,3,5-triazine-2-yl)-4-methylmorpholinium chloride (DMTMM). HA (1 g) was dissolved in 50 mL 2-(N-morpholino) ethanesulfonic acid buffer (10.0 mM, pH = 5.5). 5-Norbornene-2-methylamine solution (98.5 mg, in DMSO) and DMTMM solution (1.1 g, in DI water) was added to the above HA solution. The obtained solution was then mechanically stirred overnight and transferred into a dialysis tube (MWCO 3500, Spectrum®). After dialysis against 20 mmol NaCl solution for 2 days and then against water for 3 days. The products were frozen and lyophilized. The norbornene was determined as ~19% substitution degree by ^{1}H NMR.

The method of RGD-modified HA-NB (HA-NB-RGD) was similar to the above. Briefly, c(RGDfK) (10 mg, in DMSO) and DMTMM solution (23 mg, in water) was added simultaneously to the HA-NB solution. Then, mechanical stirred overnight and dialyzed against 20 mM NaCl solution and water for 3 days respectively. The solution was frozen and lyophilized. The c(RGDfK) was determined as ~1.8% substitution degree of HA by ^{1}H NMR.

The acquired HA-NB-RGD was dissolved in 0.1% lithium phenyl-2,4,6-trimethylbenzoyl phosphinate (LAP) solution at a concentration of 20 mg mL^{-1} with MMP-sensitive crosslinker Ac-GCRDGPQGIWGQDRCG-NH2 (H-M hydrogel) or non-degradable crosslinker SH-PEG-SH (Mw = 2000 kDa) (H–P hydrogel) followed by sterilization through filtration. Then, the two solutions were mixed in a molar ratio of norbornene and thiol at 3:2. After stirring for 30 s, 200 μL pre-solution was pipetted into 10 mm diameter and 3 mm depth Teflon disc molds before exposing to 365 nm lamp irradiation (10 mW cm^{-2}) for 1 min.

2.2. Characterization of hydrogel

Dynamic rheological analysis of the hydrogel formation process was carried out at 37 °C with a HAAKE MARS III rheometer with OmniCure Series 2000 (365 nm, 10 mW cm^{-2}). The analysis of time-sweep oscillatory was carried out at 10% strain for 180 s. The swelling ratio of gels was evaluated in PBS at 37 °C. First, the initial mass of the hydrogel was recorded (W_0). Then, samples were placed in PBS for different periods and the equilibrium wet mass (W_1) of the hydrogels at each time point was recorded. The swelling weight ratio was calculated as follows:

$$\text{Swelling weight ratio}(\%) = (W_1 - W_0) / W_0 \times 100\%$$

The degradation study was studied both by scanning electron microscope (SEM) and *in situ* rheological testing. Briefly, 0.2 mg collagenase type IV including MMPs 2 and 9, was dissolved in 400 μL PBS and mixed with hydrogels in 24 wells. SEM images of the H-M and H–P hydrogels immersed with or without enzyme solution were obtained. Meanwhile, the hydrogel modulus (G') was monitored over time by a rheometer with a parallel geometry of 20 mm.

2.3. Cell harvesting

Human vaginal fibroblasts (HVFs) were used in this study for exploring adhesive behavior on the hydrogels as being a typical regenerative cell type. HVFs were harvested from patients who approved for tissue collection and isolation. The informed consent was obtained before the isolation from the medical ethics committee of Ruijin Hospital, affiliated to the school of medicine, Shanghai Jiao Tong University. Human umbilical vein endothelial cells (HUVECs) were purchased from American type culture collection (ATCC) for *in vitro* experiments. The cells in the following experiments were cultured in DMEM (Gibco, 11885084, US). All the cells throughout the study were incubated in a CO_2 constant temperature incubator. All the cellular experiments in this study were performed in triplicate.

2.4. Cell adhesion study

To confirm the cell adhesive property of RGD modified HA-NB, the cells were digested when 80% confluence was reached and cultured on the hydrogel in a 24-well plate at 5×10^4 cells/cm^2 density. After 24 h of co-culture, paraformaldehyde (PFA) was used to fix cells. Next, after washing with PBS 3 times, Alexa Fluor 594 phalloidin was used to label cell actin and DAPI was used to label cell nuclei. Finally, confocal microscopy (LSM 800, ZEISS) and ImageJ software were used to observed cells and count the spread cells in five random areas.

Lentiviral transfection of fluorescent protein into cells. The HVFs and

HUVECs were infected with lentiviral particles carrying a red fluorescent gene (HBLV-1003, HANBIO) and green fluorescent gene (HBLV-1001, HANBIO) respectively. After infection for 48 h, the stably expressed cells were picked with the solution containing 40 μg/mL of puromycin (Life Technologies). In the presence of puromycin 3 times, the cultured cells were used in the experiments of non-cloning.

2.5. Angiogenesis assay in vitro on H-M-R hydrogel

HUVECs were seeded onto the H-M hydrogels grafted with different amounts of REG-PEG3-SH (0–0.2 mM) (H-M-R) to determine a proper concentration for following experiments through tube formation assay *in vitro*. The cell seeding process was carried as in previous studies. 80 μL of the sterilized hydrogel precursors was placed in a 24-well plate. After being exposed to UV-365 light, 6×10^4 HUVECs were seeded in each well. After labeling cell actin and nuclei in the same way mentioned above at given time points, cells were scanned both by light microscope and confocal microscopy. Image J software was used to analyze tube formation parameters.

2.6. Western blot analysis

The HUVECs seeded on the H-M-R (the concentration of REG-PEG3-SH is 0.1 mM) hydrogel were digested after 3 days of co-culture and the RIPA lysis buffer was used to extract total protein before quantified by a BCA kit. Afterward, the protein samples were electrophoresed by SDS and transferred to the PVDF membrane. Unspecific binding was blocked by 5% BSA for 2 h and was treated with primary antibodies: GAPDH (AG019, Beyotime), Hif-1α (AH339, Beyotime), VEGF (AF0312, Beyotime). Then, a secondary antibody conjugated with HRP was applied to the membranes and washed with TBST three times. Finally, the blots were visualized with a chemiluminescence detector.

2.7. PCR analysis

Trizol reagent was added to extract the total RNA of HUVEC inoculated on H-M-R. Immediately, the extracted mRNA was used to synthesize cDNA by Prime Script RT Kit (Takara, Japan). Then, SYBR Green RT-PCR Kit (Takara, Japan) was used for RT-PCR. The experiment was repeated three times and the primer sequences were as follows:

Hif-1α: Forward CCATGTGACCATGAGGAAAT
Reverse CGGCTAGTTAGGGTACACTT
VEGF: Forward TGCGGATCAAACCTCACCA
Reverse CAGGGATTTTTCTTGTCTTGCT
Gapdh: Forward ACAACTTTGGTATCGTGGAAGG
Reverse GCCATCACGCCACAGTTTC
The samples were repeated three times.

2.8. Cell scratch wound-healing assay

A 24-well plate was used for cell scratch wound-healing assay. Briefly, the RFP labeled HVFs and GFP labeled HUVECs were cultured with a density of 1×10^5 cells/well, and a wound-scratch was created with a p200 pipette tip. Then, the attached cells were cultured with the conditioned medium centrifuged the upper-medium of H–P hydrogels grafted with 0.1 mM REG-PEG3-SH (H–P-R), H-M, and H-M-R hydrogels co-cultured with macrophages (RAW, ATCC). HVFs and HUVECs were photographed after 24 h and the migration ratio was assessed through the closure area to the initial wound area and the number of migrated cells per field.

2.9. 3D cell migration assay in vitro

The HVF cell-laden rat tail collagen (C8062, Solarbio) clots were prepared as previously described. 5 μL rat tail collagen solution (2 mg mL^{-1}, 0.01MPBS) containing 1.5×10^5 cells was dropped on Teflon plate via a 1 mL syringe and placed in 37 °C incubator for 25 min. The clots were then immersed into different hydrogel precursors followed by photo-immobilization with 10 mW cm^{-2} 365 nm lamp for 30 s. After 14 days, cytoskeleton staining was performed as mentioned above and both confocal microscopy and the light microscope were used to analyze 3D cell migration behaviors. The distance of migrating cells and the migration area was measured by Image J software.

2.10. Co-culture of HVFs and HUVECs in hydrogels for 3D angiogenesis

The co-culture procedure was described as follows: all the hydrogel precursors were formulated with GFP labeled HUVECs and RFP labeled HVFs at a density of 2×10^6/mL and 1×10^6/mL respectively exposed to 365 nm lamp to photo-induced gelation. The cells encapsulated in hydrogels were incubated in the same way mentioned above and the angiogenic capabilities were tested at given time points. Since the cells were rendered fluorescence already, the nuclei were labeled alone and observed under confocal microscopy for 3D tube formation assay. The number of junctions and total length of the tube were calculated by Image J software.

2.11. Rat skin defect model

A full-thickness excisional skin defect model was adopted mainly to investigate the potential of functional hydrogel on soft tissue wound healing. The experimental process was carried out according to the regulations of the Animal Ethics Committee of Shanghai Ruijin Hospital. The seventy-two male SD rats (two months old, 200 g) were injected with pentobarbital sodium solution and removed back hair, two full-thickness round skin wounds with 10 mm diameter were excised from the back of each rat. The 200 μL sterilized hydrogel pre-solution was injected via a 1 mL syringe right onto the skin defect and followed by a 365 nm UV lamp exposure for 30 s to immobilize the hydrogels. Then, covered dressings were sutured to fix the implants in place. Then, the animals were monitored daily. The control group treated with PBS was also undergoing the same protection process to eliminate environmental differences. Finally, at 3, 7, and 14 days, the animals were sacrificed. After taking photographs of the injury sites, tissue samples were obtained and maintained in a 4% PFA for histological studies ($n = 6$). Hematoxylin and eosin (H&E) and immunofluorescent staining including Col Iα (ab34710, Abcam), α-SMA (1A4, ab7817), and CD31 (ab182981) were used to explore collagen deposition and neovascularization. To detect the inflammatory cells in the explanted grafts, mouse anti CD68 antibody (1:100, Abcam,ab31630) was used. Rabbit anti-INOS antibody (1:70, Abcam, ab15323) and anti-Mannose Receptor antibody (1:200, Abcam, ab64693) were used to identify M1 and M2 macrophages, respectively.

2.12. Mouse skin random flap model

48 male mice, eight weeks old (Shanghai SLAC Laboratory Animal Co. Ltd) for the experiment. The mice were randomly divided into the group of control, H–P-R, H-M, and H-M-R. Primarily, after being sterilized, the mice were anesthetized, and a 10 mm × 40 mm/width × length full-thickness skin flap was created. Before the flap was carefully sutured back, 10 μL of each group hydrogel or PBS as control was injected intradermally into each flap from distal to the pedicle. After the surgery, mice were sent back to the cages.

After 7 days of treatment, the surviving and necrotic areas of the random skin flaps were photographed, the necrotic area of the flaps was determined by the skin color, appearance, tissue texture, and the moor FLPI blood flow imager (Moor Instruments, Axminster, UK) with laser speckle contrast was used to capture the real-time blood flow images. The necrotic area was quantified with the following equation:

$$\text{Necrotic area}(\%) = \text{necrotic skin area}/\text{total flap area} \times 100\%$$

On day 7 and day 14 after the surgery, 1 cm × 1 cm specimens were harvested from the junction areas of the necrosis and survival for histological assessment. After extraction, all tissue was fixed with 4% PFA for 48 h. To analyze angiogenesis efficacies of the hydrogel, HE staining and immunofluorescent staining including α-SMA (ab5694), and CD31 (ab182981) were performed.

2.13. Statistical analysis

Data were performed with a *t*-test, one- or two-way ANOVA analysis of variance with a post-test, which was used to examine the differences among variables. And all data were shown as mean ± SD. All statistical quantifications were using ImageJ software on high-resolution images and GraphPad Prism Software. *P < 0.05 were considered statistically significant.

3. Results and discussion

To initiate the early repair process, an MMPs sensitive hydrogel system was designed in this work to meet the inflammatory microenvironment triggered degradation [31]. Hyaluronic acid (HA), an important component of natural ECM, was chosen as the skeleton of hydrogel for followed reasons: 1) HA has excellent biocompatibility and low immunogenicity. 2) HA itself lacks complex biological cues though, the polymer network is rich in hydroxyl and carboxyl groups and can be customized into different biochemical signals [32,33]. Firstly, a bifunctional hyaluronic acid HA-NB-RGD was synthesized (Fig. 2a, Figs. S1-S3, Supporting Information), including norbornene which can carry out a rapid and highly specific thiol-ene click reaction and a fibronectin-derived adhesion peptide cyclo(Arg-Gly-Asp-D-Phe-Lys) c (RGDfK). A dicysteine peptide (Ac-GCRDGPQG↓IWGQDRCG-NH2, ↓ represents the cleavage site) was chosen as the crosslinker which is sensitive to MMPs 1, 2, 3, 7, 8, and 9 [34,35]. Meanwhile, a non-degradable cross-linking agent dicysteine PEG (SH-PEG-SH, Mw = 2000 Da) was selected as control. The off-stoichiometric ratio of thiol (SH) to norbornene (NB) was fixed at 3:2 (NB: SH = 3:2) to facilitate the functionalization of subsequent biochemical signal molecules. As shown in Fig. 2b, the rheological behavior of hydrogels was analyzed upon 365 nm (10 mW cm^{-2}) exposure, the MMPs-degradable hydrogel (H-M) and the non-degradable hydrogel (H–P) formed within 5 s (Fig. S3b, Supporting Information), and there was no significant difference in storage modulus (G') and swelling ratio (Fig. 2c) between the two groups.

To investigate inflammatory mediator MMPs responsive degradation, the scanning electron microscopic (SEM) morphology and rheological properties were measured after treated with collagenase type IV (a mixture of MMP2 and MMP9). As observed from Fig. 2d ~ e, the

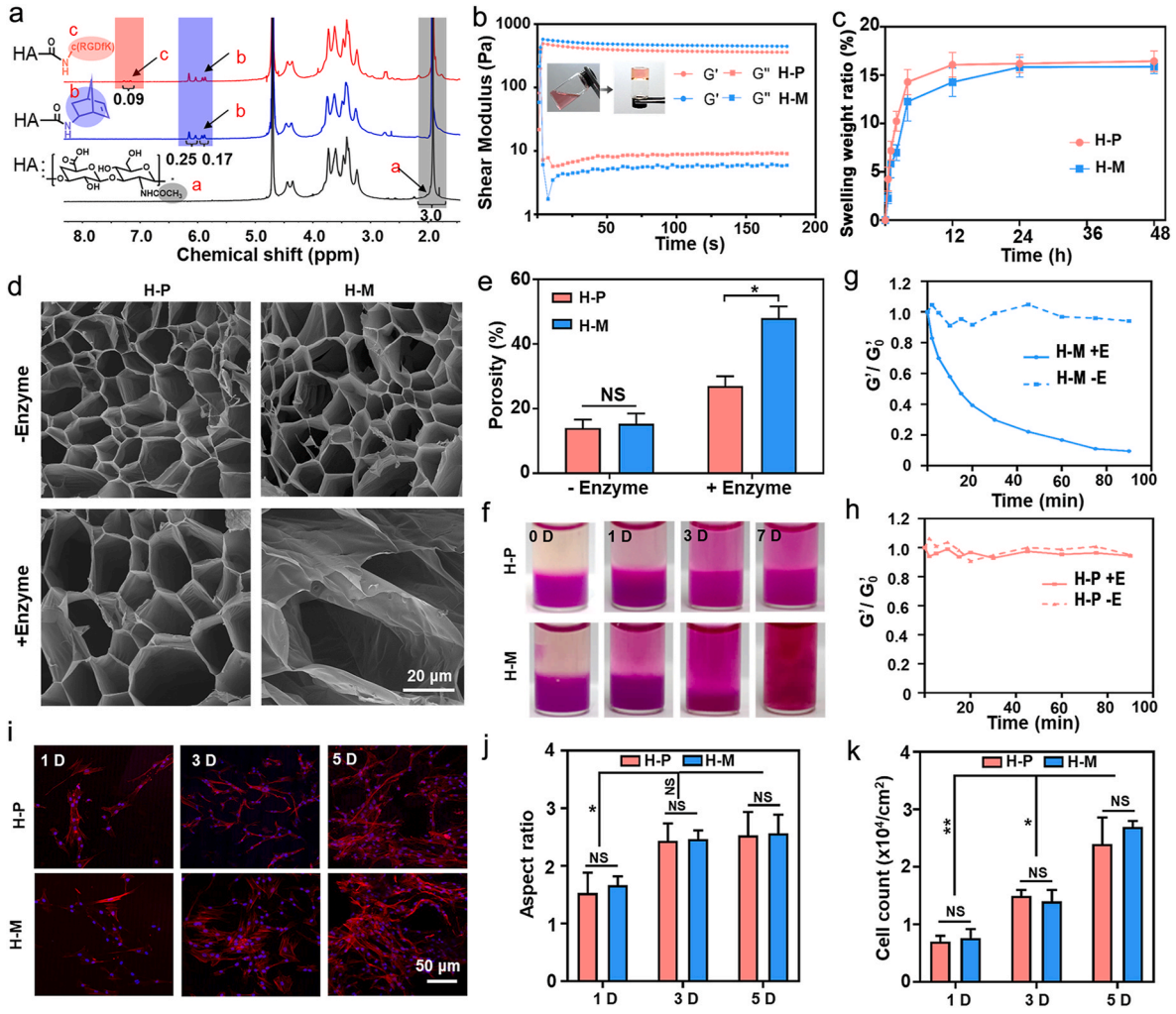

Fig. 2. Synthesis, characterization, and biocompatibility of MMPs sensitive hydrogels for Phase I. a) ^{1}H NMR spectrum analysis (600 MHz, D_2O) of HA, HA-NB, and HA-NB-RGD. b) Rheology analysis and a photograph of hydrogel formation for HA-NB-RGD with MMP-cleavable crosslinker SH-MMP-SH (H–M) or non-degradable crosslinker SH-PEG-SH (H–P) (SH: NB = 2:3). c) Swelling weight ratio. SEM analysis d), porosity analysis e), photograph visualization f) and rheological analysis of H-M g) and H–P h) hydrogel degradation. Cytoskeleton staining i), cell aspect ratio j) and cell count k) of the HFVs on the H–P and H-M hydrogel.

physical morphology of H-M was much looser than H–P after treatment and the porosity of H-M reached 47.5 ± 2.3%, much higher than 21 ± 1.9% of H–P. Also, the H-M network was collapsed completely while the H–P still maintained its integral gel morphology after soaked in collagenase type IV buffer for 7 days (Fig. 2f). Besides, the rheological studies over time demonstrated that the storage modulus of H-M decreased significantly after the addition of collagenase IV, which was in deep contrast with H–P (Fig. 2g and h). Overall, it was confirmed that the H-M was responsive to the inflammatory mediator MMPs, and with the decreased cross-linking density and the increased porosity, which would provide sufficient dynamic physical space during the precise soft tissue remodeling.

Furthermore, the cell anchoring and survival on H-M hydrogel were studied *in vitro*. Two-dimensional (2D) cell adhesion experiments were conducted to verify the cellular adhesive property of RGD. Few cells survived on the surface of HA-NB hydrogel without RGD (Fig. S4, Supporting Information), and as expected, after the c(RGDfK) modification, good adhesion and spreading were observed and the number of cells on the hydrogel increased with the culture time. Interestingly, from Fig. 2i–k, it could be concluded that the degradability of the hydrogels did not affect the aspect ratio of cells and cell proliferation, indicating that the proliferation of cells on the 2D surface was not limited by the three-dimensional (3D) space of the hydrogel.

To testify the recruitment and regulation of regenerative cells which is supposedly triggered by the chemotaxis of hydrogel degradation, controlled migrative modulations in the hydrogel are further studied [36]. Specifically, a thiol-modified chemotactic active peptide (SH-PEG3-REG) was used to improve the residence time of the active peptide through the thiol-ene click reaction and maintain the chemotactic activity of the hydrogel. To prove the successful modification of active peptide, photolithographic techniques and rhodamine B labeled active peptide was used for fluorescent imaging. It was shown that the fluorescence was different between the regions of irradiated and nonirradiated, and 3D patterns were continuous in the bulk hydrogel demonstrating the efficient grafting of the active peptide in the hydrogel (Fig. S5, Supporting Information). As shown in Fig. 3a–c and Fig. S5b, H-M hydrogels grafted with REG (H-M-R), matrix chemotaxis indeed induced the endothelial cell migration and vascular tube formation.

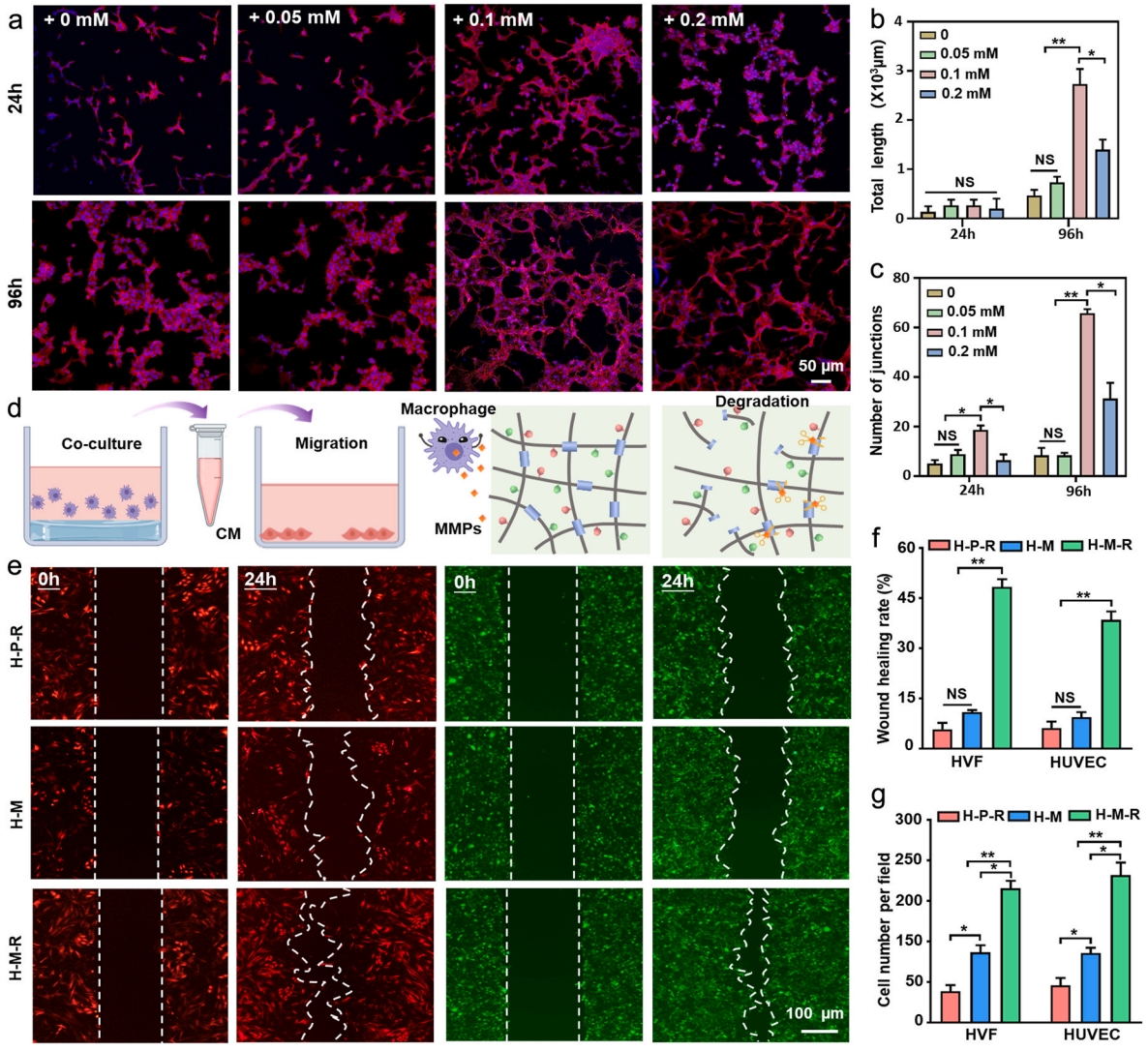

Fig. 3. *In vitro* cell angiogenesis and cell migration activity analysis of chemokine-like hydrogels for Phase II. a) The confocal images of vascular tube-formation with HUVEC at 24 h and 96 h after culturing on H-M hydrogel grafted with different concentrations of chemokine-like peptide. Quantification of total length (b) and the number of junctions (c). d) Schematic diagram showing the co-culture model of macrophages with H-M/H–P hydrogel grafted with 0.1 mM REG-PEG3-SH (H-M-R or H–P-R hydrogel) to form a conditioned medium (CM) for cell migration and the mechanism of the hydrogel degradation with macrophages. e) HVF (red) and HUVEC (green) wound scratch assay with H-M, H–P-R, and H-M-R hydrogel conditioned medium. Quantification of the wound healing rate f) and cell number g) of migrated cells. *p < 0.05, **p < 0.01.

After 96 h of culture, the junction points of endothelial cells reached the highest point together with a tube length of 2 ± 0.4 mm when the concentration of REG was reached at 0.1 mM, while much fewer junction points were observed within the lower or higher REG concentrations indicating that the optimal concentration of REG should be 0.1 mM. Given that, the concentration was chosen for both the following *in vitro* and *in vivo* experiments. Furthermore, we studied the underlined mechanism of functional peptide REG for promoting angiogenesis through WB and RT-PCR (Fig. S6, Supporting Information). The results showed that this peptide realized neovascularization by activating the hypoxia-inducible factor-1α (HIF-1α) pathway as the main signal molecules presented a high expression rate both from protein and gene levels.

Next, the effect of H-M-R degradation products on the migration of fibroblasts and endothelial cells was explored to determine whether the small active peptides still maintain chemotactic activity after covalently grafted. For this purpose, macrophages (RAW, ATCC) were used to simulate the early inflammatory microenvironment triggered H-M-R degradation (Fig. 3d), H-M and REG grafted H–P peptides (H–P-R) as control groups, and the degradation product's migration efficacy of regenerative cells was conducted through the standard *in vitro* scratch wound healing test (Fig. 3e). The results given in Fig. 3f and g showed that after 24 h of co-culture, compared with control ones, the grafted REG effectively promoted the migration of fibroblasts and endothelial cells both from the perspectives of wound healing rate and migrated cell number per observed field.

During the subacute repairing phase of injury soft tissues such as muscle, fascia, as well as skin, neovascularization can improve the microcirculation and provide nutrition for tissue regeneration. Angiogenesis is achieved through the complex interactions of endothelial cells, ECM, and the adjacent cells through a variety of growth factors. The most first step, however, is to promote the migration of regenerative cells to the wound site in a complex microenvironment [37,38]. Given that, we confirmed the cell migration function of H-M-R in a 3D cell invasion model *in vitro*. The fibroblasts-laden collagen clots were successfully encapsulated into the hydrogel systems and cytoskeleton staining was performed to track the morphogenesis of cells. The encapsulated fibroblasts exhibited different migration behavior in the

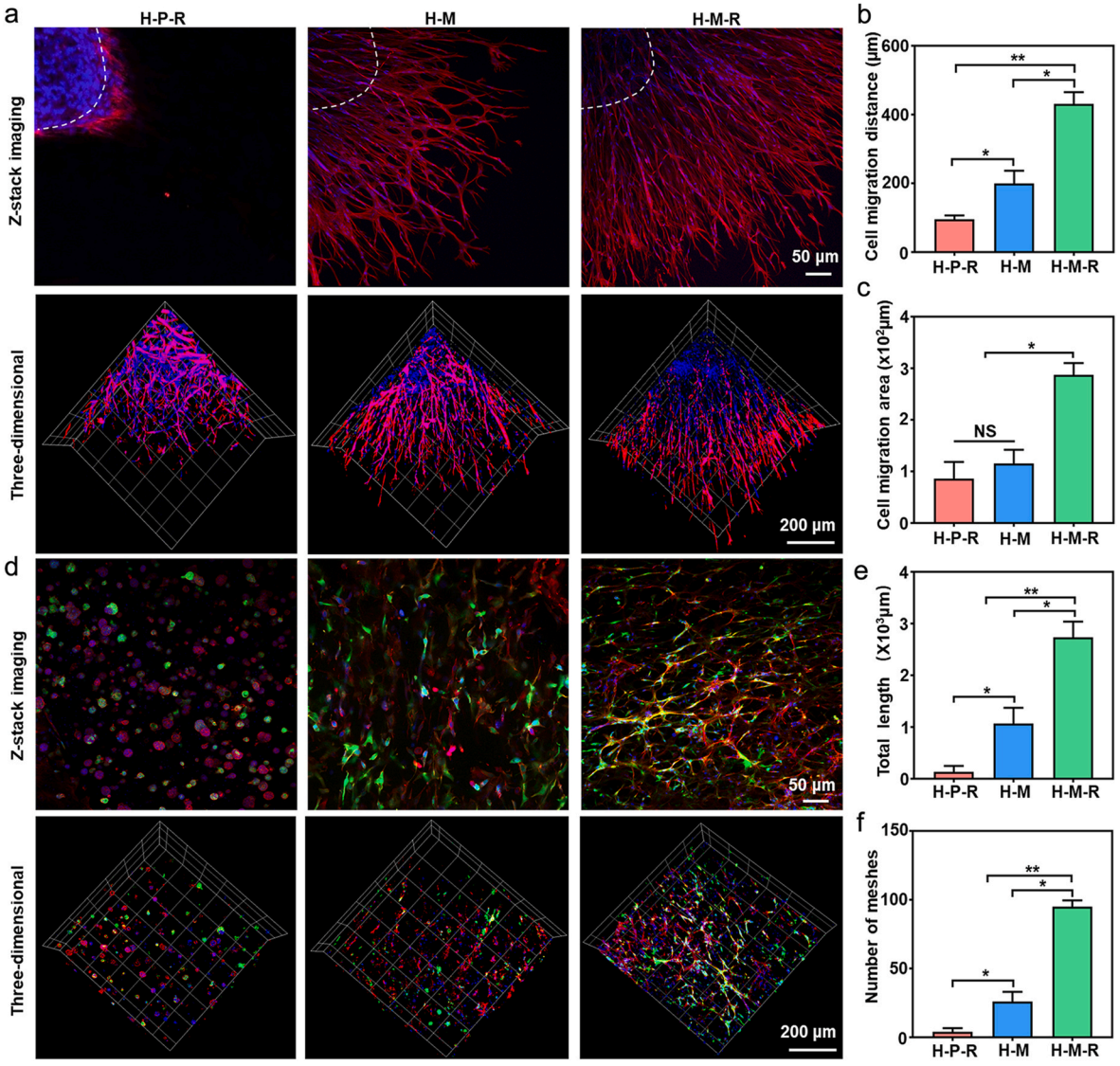

Fig. 4. Cell invasion and tubule formation in 3D hydrogels for Phase III. a) Z-stack and 3D confocal images of actin/nuclei (red/blue) stained HVF clusters encapsulated in H–P-R hydrogel (non-degradable, adhesive, and chemotactic), H-M hydrogel (degradable and adhesive), and H-M-R hydrogel (degradable, adhesive, and chemotactic) cultured for 14 d. And the quantification of the cell migration distance b) and cell migration area c). d) Z-stack and 3D confocal images of HVFs (red) and HUVECs (green) co-cultured in H–P-R, H-M, and H-M-R hydrogels for 14 days. e, f) The quantification of total length and number of meshes. *$p < 0.05$, **$p < 0.01$.

hydrogels after 7d of co-culture (Fig. 4a, Fig. S7, Supporting Information). Cells in H-M-R exhibited higher viability and spindle-like morphology. Fig. 4b and c illustrated that the cells in the H-M-R group showed much further migration distance (404 ± 19 μm) and higher spreading areas (2.7×10^2 μm^2) than the results being 90 ± 11 μm, 199 ± 21 μm, and 0.8×10^2 μm^2, 1.1×10^2 μm^2 respectively as for undegradable H–P-R and H-M that without REG. These results demonstrated that both the degradability and the chemotaxis are necessary for regenerative cells to migrate and keep normal morphogenesis which is essential for the tissue healing process.

To investigate new blood vessel formation in 3D hydrogels, the heterotypic cell interactions between HUVECs and fibroblasts were explored. Although HUVECs can build primitive tubular networks when cultured alone, the interaction with mural cell types will be required for the newly formed blood vessels to become mature. Fibroblasts are typical pericytes that are known to support the formation of endothelial tubules. In the H-M-R group, HUVECs and fibroblasts formed primitive tubular networks by day 7 in the 3D hydrogels matrix (Fig. S8, Supporting Information). However, in the H–P-R group, the tubular formation was decreased because cells could not migrate as much as that in MMPs sensitive hydrogel (Fig. 4d–f). In contrast, the number of meshes and total length reached 93 ± 4 and 2.6×10^3 μm respectively. Collectively, these data demonstrated that regenerative cells could dynamically remodel their microenvironments in the HA matrix with cell-mediated degradation and the dynamic interactions through various biological signals.

The chronic remodeling phase was further evaluated through a rat full-thickness excisional wound model and a mice skin flap regeneration

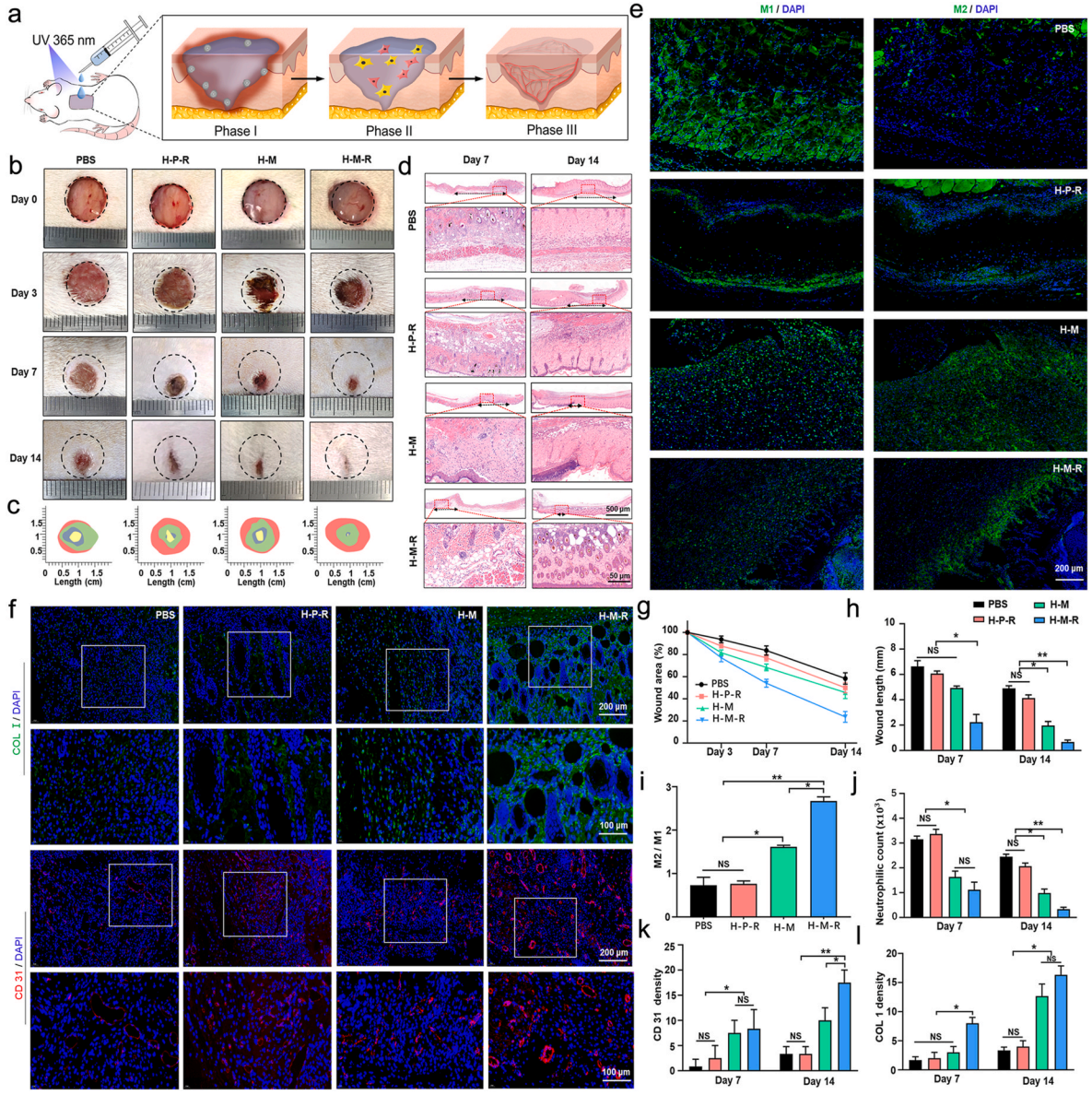

Fig. 5. Bio-mimicking hydrogel promoted wound healing *in vivo* by matching the different phases of soft tissue regeneration. a) The schematic diagram illustrating the mechanism of accelerating wound closure based on H-M-R hydrogel (n = 6). b) The representative photographs of wound healing of rats treated with PBS, H–P-R, H-M, and H-M-R hydrogels treatments on days 0, 3, 7, 14. c) Wound closure boundaries during 14 days *in vivo* for each treatment. d) HE stained sections of skin tissue on days 7 and 14 (above: cross-section; below: longitudinal section), the black arrow means the length of the wound in the HE staining. e) Immunofluorescence images of explanted samples stained for, iNOS (M1), CD206 (M2). f) The immunofluorescence staining for Col I and CD31(CD31-positive endothelial cells) at 14 days. g, h) Wound area and length of each group at different time points. i) The ratio of M2/M1 macrophages in all groups on day 3. j) The quantification of neutrophilic cells of different groups at 7 and 14 days. k, l) The quantification of immunofluorescence intensity of Col I and α-SMA at 7 and 14 days. *p < 0.05, **p < 0.01.

in vivo. The operation and healing process of skin full-thickness wound is presented in Fig. 5a. During the whole treatment(Fig. 5b), the healing trend among the four groups was consistent (Fig. 5c, Fig. S9, Supporting Information), for the H-M-R group, due to the existence of chemotactic peptide REG, the wound area (53.2 ± 1.6%) significantly decreased compared with control (83.6 ± 2.3%), H–P-R (81.1 ± 2.7%), and H-M (78.9 ± 1.8%) groups on day 7. As the treatment progressed, the wound area in each group gradually reduced, and 16.6 ± 1.3% of wound area was left in the H-M-R group on day 14 (Fig. 5g), compared with that in control (52.2 ± 1.0%), H–P-R group (49.5 ± 2.2%) and H-M group (46.7 ± 1.6%). The wound samples were harvested at a predesigned time point and reserved in the PFA. After first-week treatment, almost no epidermis structure was found in the control group as well as the H–P-R and H-M groups, but there was obvious regenerated epidermis in the H-M-R group (Fig. 5d). Besides, the wound defect was almost healed after 14 days of treatment with H-M-R hydrogel, while a larger defect still

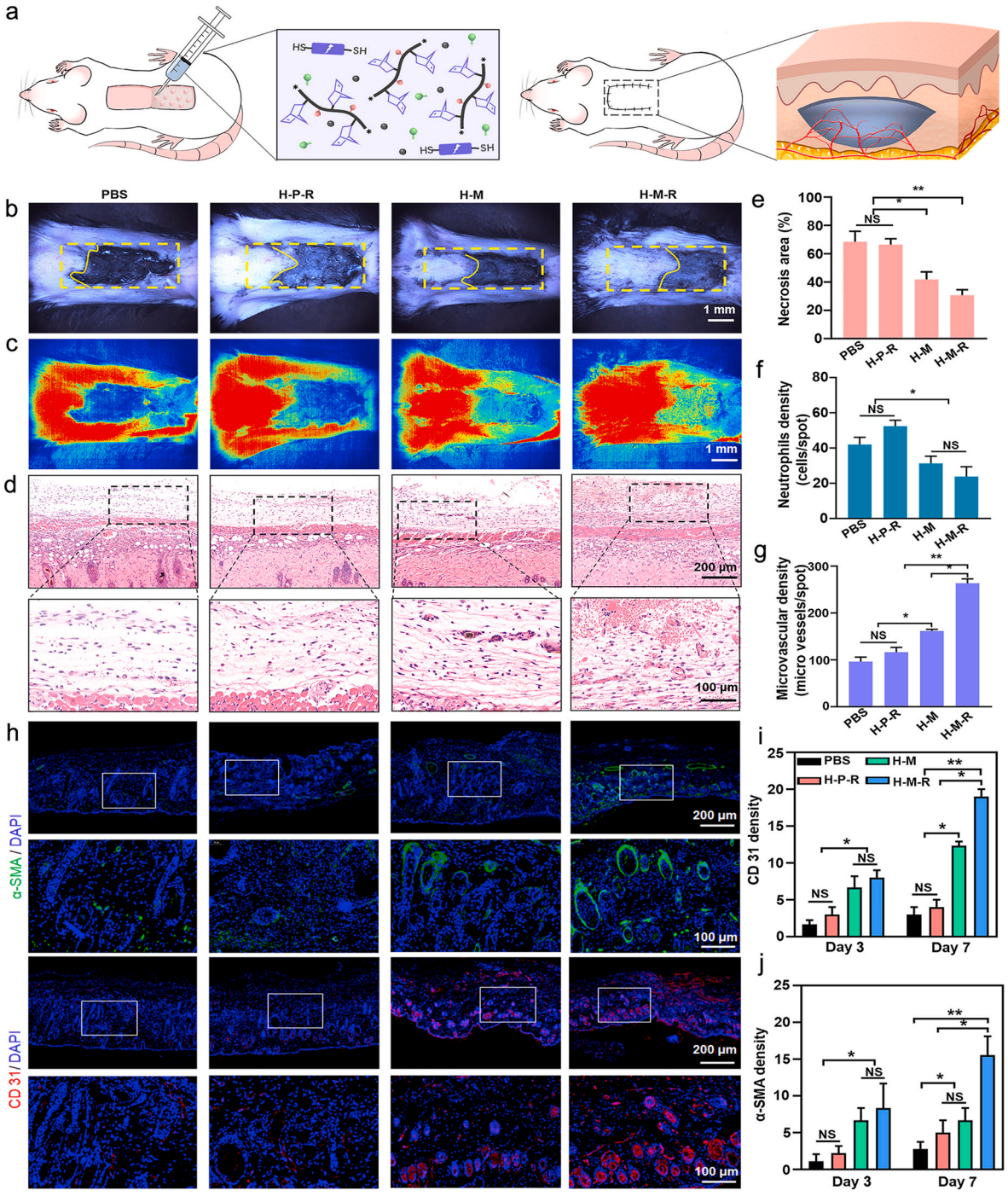

Fig. 6. Bio-mimicking hydrogel promoted skin flap angiogenesis and regeneration. a) Schematic diagram of hydrogel injection below skin flap (n = 6). b) Photographic images of a necrotic area in the flaps. c) The real-time blood flow images of each group at days 7 were detected with laser speckle contrast. The Red signal represents the perfusion of blood perfusion. d) H&E staining sections of the junction of skin flap necrosis and survival in each group at days 7. e) The necrosis area proportion of flaps in different groups. f, g) The quantification of the neutrophilic density and microvascular density in different groups. h) Images of immunofluorescence staining for α-SMA and CD31 at 7 days. And the quantification of immunofluorescence intensity of α-SMA i) and CD31 j) at 3 and 7 days. *p < 0.05, **p < 0.01.

sustained without obvious epidermal tissue structure in the other three groups (Fig. 5h).

Since our bio-mimicking hydrogel was designed following the inflammatory response, we further analyzed one of the important early inflammatory indicators—macrophages. Macrophages can be divided into pro-inflammatory type (M1) or anti-inflammatory type (M2) macrophage during tissue regeneration. Immunofluorescence staining in Fig. 5e, i showed that in the H-M-R group, the fluorescence intensity expression of iNOS (M1 marker) was significantly lower than other groups on day 3, and while the fluorescence intensity level of CD206 (M2 marker) was higher than other groups. The ratio of M2/M1 ratio, an indicator of regeneration, was calculated according to the fluorescence intensity. As shown in Fig. 5j, the M2/M1 ratio was increased significantly which demonstrated the regenerative potential of the H-M-R rather than the inflammation trend. In addtion, the neutrophils number increased in all groups on day 7 but the H-M and H-M-R groups presented much fewer inflammatory cells than the control and H–P-R groups mainly due to the existence of degradable linker and cell adhesive peptide. However, on day 14, the neutrophils reduced sharply in the H-M-R group confirming its wound healing efficacy.

Furthermore, immunofluorescent staining to detect collagen deposition in the injury site was studied. Collagen I (COL I), being the major constructive part of the skin, can help repair the injured tissues both structurally and functionally [39]. As the time increased, much more COL I deposition was detected in the H-M-R group (Fig. 5f, i). At 14 day, granulation tissue of the wound was nearly replaced with collagen in the H-M-R group, the immunofluorescence intensity of COL I was almost 10 times higher than the control group (Fig. S10, Supporting Information). The new capillaries in the injured site were crucial for wound repair, which can provide nutrition to damaged tissue. The neovascularization of the H-M-R hydrogel was evaluated by fluorescent staining of endothelial cells and smooth muscle cells. In Fig. 5d, i, on day 7, few new blood vessels were obvious in all four groups, but the number of vessels in the H-M-R group was significantly more than that in the other three groups on day 14, which was mainly attributed to the vascularization ability of chemokine-like peptide. On day 14, the fluorescence intensity of CD31 and α-SMA in H-M-R group reached the peak. Conversely, the expression of CD31 and α-SMA was very low in the control group (Fig. 5f, k). These results indicated that bio-mimicking hydrogel can effectively regulate early inflammation, recruit peripheral cells, promote collagen deposition and angiogenesis, and realize precise skin remodeling.

To further demonstrate the precise soft tissue regeneration ability of the bio-mimicking hydrogel *in vivo*, the random skin flap model was investigated. The hydrogel was injected randomly into the skin flap and returned to its original position to promote the regeneration of new blood vessels from the adjacent area to the distal end of the skin flap (Fig. 6a, Fig. S11, Supporting Information). On day 7, the mice were anesthetized, and the real-time blood flow of the skin flap was detected with moor full-field laser perfusion imaging (FLPI). The contrast images color-coded were obtained, which is related to the blood flow of the flap (Fig. 6b and c). As for the H-M-R group, the necrosis ratio of the flap was decreased significantly by 31 ± 2% (n = 6) compared to the control group (68 ± 5%), H–P-R group (66.6 ± 2%), and H-M groups (41 ± 3%) (Fig. 6e). It can be concluded that the bio-mimicking hydrogel is of great significance in promoting blood perfusion and remodeling of skin flap in mice. Moreover, from HE staining results it could be seen that no hydrogel was observed in the flap due to the little size and rapid degradation of hydrogels (Fig. 6d) [40]. To evaluate the local inflammatory reaction of hydrogel and its phase-based remodeling potential, the neutrophils and newly formed microvascular density were calculated in Fig. 6f and g. It showed that a lower inflammatory cell accumulation and more increased microvascular density in the H-M-R group compared to the other three groups, which significantly increased the survival rate of skin flap distal end. These results indicate that bio-mimicking hydrogel will not aggravate the original inflammation of damaged soft tissue in the process of regeneration.

Finally, immunohistochemical staining was performed to further explore the effect of bio-mimicking hydrogel on the angiogenesis of skin flap [41,42]. On day 7, the average microvessel densities were marked with CD31, 96.3 ± 10 microvessels/spot in the control group; 110.6 ± 9 microvessels/spot in the H–P-R group; 161.2 ± 4 microvessels/spot in the H-M group; 263 ± 11 microvessels/spot in the H-M-R group; as for α-SMA, the trend was the same as CD31. It revealed that the H-M-R hydrogel capturing dynamic biological signals significantly promoted regeneration of flap microvessels (Fig. 6h, i, j and Fig. S12, Supporting Information). All these results confirmed that the H-M-R bio-mimicking hydrogel had a strong potential to accelerate precise soft tissue remodeling and inflammatory regulation.

4. Conclusions

In this study, we innovatively constructed a bio-mimicking hydrogel to capture dynamic biological signals that the early triggered degradation of inflammation, the recruitment activity of chemokines, and the colonization efficiency of natural adhesion sites for precise soft tissue remodeling. Phase I: the enzymatic degradation experiment verified that the inflammatory mediator responsive characteristic of the hydrogel. Phase II: 2D cell wound scratch study confirmed that the recruitment activity of hydrogel degradation products. Phase III: cell invasion and vascular network formation in 3D hydrogel demonstrated that the colonization and the interactions of cell-matrix and cell-cell in the hydrogel system. In addition, the rat skin acute wound and mouse skin flap regeneration models revealed the macrophage polarization, collagen deposition and angiogenesis, and eventually the precise regeneration of the damaged soft tissue. In conclusion, the capturing dynamic biological signals' hydrogel achieved precise remodeling of soft tissue and put forward a new horizon for the phased precise repair of different tissues.

CRediT authorship contribution statement

Zhengwei Cai: Conceptualization, Methodology, Investigation, Formal analysis, Writing – original draft. **Qimanguli Saiding:** Investigation, Conducted the animal experiments, Formal analysis, Writing – review & editing. **Liang Cheng:** Resources, Conducted the animal experiments, Formal analysis. **Liucheng Zhang:** Visualization, Data curation. **Zhen Wang:** Investigation, Writing – review & editing. **Fei Wang:** Methodology, Writing – review & editing. **Xinliang Chen:** Visualization, Resources. **Gang Chen:** Resources, Funding acquisition. **Lianfu Deng:** Supervision, Project administration. **Wenguo Cui:** Conceptualization, Writing – original draft, Funding acquisition, Project administration, Resources, Supervision.

Declaration of competing interest

The authors declare no conflict of interest.

Acknowledgments

Dr. Z. Cai, Dr. Q. Saiding contributed equally to this work. This research was funded by The National Key Research and Development Program of China (2020YFA0908200), National Natural Science Foundation of China General Program (81930051), Postdoctoral Research Foundation of China (2020M681319), the Interdisciplinary Program of Shanghai Jiao Tong University (YG2019ZDA05 and ZH2018ZDA04), "The Project Supported by the Foundation of National Facility for Translational Medicine (Shanghai) (TMSK-2020-117)" and Shanghai Municipal Education Commission—Gaofeng Clinical Medicine Grant Support (20171906).

Appendix A. Supplementary data

Supplementary data to this article can be found online at https://doi.org/10.1016/j.bioactmat.2021.04.039.

References

[1] X. Li, B. Cho, R. Martin, M. Seu, C. Zhang, Z. Zhou, J.S. Choi, X. Jiang, L. Chen, G. Walia, J. Yan, M. Callanan, H. Liu, K. Colbert, J. Morrissette-McAlmon, W. Grayson, S. Reddy, J.M. Sacks, H.Q. Mao, Nanofiber-hydrogel composite–mediated angiogenesis for soft tissue reconstruction, Sci. Transl. Med. 11 (490) (2019), eaau6210.

[2] R. Raghow, The role of extracellular matrix in postinflammatory wound healing and fibrosis, Faseb. J. 8 (11) (1994) 823–831.

[3] P. Olczyk, K. Mencner, K. Komosinska-Vassev, The role of the extracellular matrix components in cutaneous wound healing, BioMed Res. Int. 2014 (2014), 747584.

[4] B.V. Slaughter, S.S. Khurshid, O.Z. Fisher, A. Khademhosseini, N.A. Peppas, Hydrogels in regenerative medicine, Adv. Mater. 21 (2009) 3307–3329.

[5] Y.S. Zhang, A. Khademhosseini, Advances in engineering hydrogels, Science 356 (2017), eaaf3627.

[6] M. Lee, R. Rizzo, F. Surman, M. Zenobi-Wong, Guiding lights: tissue bioprinting using photoactivated materials, Chem. Rev. 120 (19) (2020) 10950–11027.

[7] S. Cascone, G. Lamberti, Hydrogel-based commercial products for biomedical applications: a review, Int. J. Pharm. 573 (2020), 118803.

[8] S.H. Aswathy, U. Narendrakumar, I. Manjubala, Commercial hydrogels for biomedical applications, Heliyon 6 (4) (2020), e03719.

[9] C.C. Lin, K.S. Anseth, PEG hydrogels for the controlled release of biomolecules in regenerative medicine, Pharm. Res. (N. Y.) 26 (3) (2009) 631–643.

[10] W.D. Spotnitz, S. Burks, Hemostats, sealants, and adhesives III: a new update as well as cost and regulatory considerations for components of the surgical toolbox, Transfusion 52 (10) (2012) 2243–2255.

[11] S. Chattopadhyay, R.T. Raines, Collagen-based biomaterials for wound healing, Biopolymers 101 (8) (2014) 821–833.

[12] T.A.E. Ahmed, E.V. Dare, M. Hincke, Fibrin: a versatile scaffold for tissue engineering applications, Tissue Eng. B Rev. 14 (2) (2008) 199–215.

[13] C. Nathan, Points of control in inflammation, Nature 420 (6917) (2002) 846–852.

[14] C. Nathan, A. Ding, Nonresolving inflammation, Cell 140 (6) (2010) 871–882.

[15] W.C. Parks, C.L. Wilson, Y.S. López-Boado, Matrix metalloproteinases as modulators of inflammation and innate immunity, Nat. Rev. Immunol. 4 (8) (2004) 617–629.

[16] J.M. Anderson, A. Rodriguez, D.T. Chang, Foreign body reaction to biomaterials, Semin. Immunol. 20 (2) (2008) 86–100.

[17] K. Sadtler, M.T. Wolf, S. Ganguly, C.A. Moad, L. Chung, S. Majumdar, F. Housseau, D.M. Pardoll, J.H. Elisseeff, Divergent immune responses to synthetic and biological scaffolds, Biomaterials 192 (2019) 405–415.

[18] B.A. Badeau, C.A. DeForest, Programming stimuli-responsive behavior into biomaterials, Ann. Rev. Biomed. En. 21 (1) (2019) 241–265.

[19] D.R. Griffin, W.M. Weaver, P.O. Scumpia, D. Di Carlo, T. Segura, Accelerated wound healing by injectable microporous gel scaffolds assembled from annealed building blocks, Nat. Mater. 14 (7) (2015) 737–744.

[20] C. Gerard, B.J. Rollins, Chemokines and disease, Nat. Immunol. 2 (2) (2001) 108–115.

[21] M. Martins-Green, M. Petreaca, L. Wang, Chemokines and their receptors are key players in the orchestra that regulates wound healing, Adv. Wound Care 2 (7) (2013) 327–347.

[22] B.P. Purcell, J.A. Elser, A. Mu, K.B. Margulies, J.A. Burdick, Synergistic effects of SDF-1α chemokine and hyaluronic acid release from degradable hydrogels on directing bone marrow derived cell homing to the myocardium, Biomaterials 33 (31) (2012) 7849–7857.

[23] B.P. Purcell, I.L. Kim, V. Chuo, T. Guenin, S.M. Dorsey, J.A. Burdick, Incorporation of sulfated hyaluronic acid macromers into degradable hydrogel scaffolds for sustained molecule delivery, Biomater. Sci. 2 (5) (2014) 693–702.

[24] J.L. Lau, M.K. Dunn, Therapeutic peptides: historical perspectives, current development trends, and future directions, Bioorg. Med. Chem. 26 (10) (2018) 2700–2707.

[25] S.Y. Wang, H. Kim, G. Kwak, H.Y. Yoon, S.D. Jo, J.E. Lee, D. Cho, I.C. Kwon, S. H. Kim, Development of biocompatible HA hydrogels embedded with a new synthetic peptide promoting cellular migration for advanced wound care management, Adv. Sci. 5 (11) (2018) 1800852.

[26] G.S. Hussey, J.L. Dziki, S.F. Badylak, Extracellular matrix-based materials for regenerative medicine, Nat. Rev. Mater. 3 (7) (2018) 159–173.

[27] Y. Xu, G. Shi, J. Tang, R. Cheng, X. Shen, Y. Gu, L. Wu, K. Xi, Y. Zhao, W. Cui, L. Chen, ECM-inspired micro/nanofibers for modulating cell function and tissue generation, Sci. Adv. 6 (48) (2020), eabc2036.

[28] M.P. Lutolf, J.A. Hubbell, Synthetic biomaterials as instructive extracellular microenvironments for morphogenesis in tissue engineering, Nat. Biotechnol. 23 (1) (2005) 47–55.

[29] O. Chaudhuri, L. Gu, D. Klumpers, M. Darnell, S.A. Bencherif, J.C. Weaver, N. Huebsch, H.-p. Lee, E. Lippens, G.N. Duda, D.J. Mooney, Hydrogels with tunable stress relaxation regulate stem cell fate and activity, Nat. Mater. 15 (2015) 326.

[30] N. Gjorevski, N. Sachs, A. Manfrin, S. Giger, M.E. Bragina, P. Ordonez-Moran, H. Clevers, M.P. Lutolf, Designer matrices for intestinal stem cell and organoid culture, Nature 539 (7630) (2016) 560–564.

[31] Q. Chen, M. Jin, F. Yang, J. Zhu, Q. Xiao, L. Zhang, Matrix metalloproteinases: inflammatory regulators of cell behaviors in vascular formation and remodeling, Mediat. Inflamm. 2013 (2013), 928315.

[32] J. Liang, D. Jiang, P.W. Noble, Hyaluronan as a therapeutic target in human diseases, Adv. Drug Deliv. Rev. 97 (2016) 186–203.

[33] M.N. Collins, C. Birkinshaw, Hyaluronic acid based scaffolds for tissue engineering—a review, Carbohydr. Polym. 92 (2) (2013) 1262–1279.

[34] M.P. Lutolf, J.L. Lauer-Fields, H.G. Schmoekel, A.T. Metters, F.E. Weber, G. B. Fields, J.A. Hubbell, Synthetic matrix metalloproteinase-sensitive hydrogels for the conduction of tissue regeneration: engineering cell-invasion characteristics, Proc. Natl. Acad. Sci. Unit. States Am. 100 (9) (2003) 5413.

[35] Z. Cai, K. Huang, C. Bao, X. Wang, X. Sun, H. Xia, Q. Lin, Y. Yang, L. Zhu, Precise construction of cell-instructive 3D microenvironments by photopatterning a biodegradable hydrogel, Chem. Mater. 31 (13) (2019) 4710–4719.

[36] X. Zheng, S. Narayanan, V.G. Sunkari, S. Eliasson, I.R. Botusan, J. Grünler, A. I. Catrina, F. Radtke, C. Xu, A. Zhao, N.R. Ekberg, U. Lendahl, S.-B. Catrina, Triggering of a Dll4–Notch1 loop impairs wound healing in diabetes, Proc. Natl. Acad. Sci. Unit. States Am. 116 (14) (2019) 6985.

[37] K. Sadtler, A. Singh, M.T. Wolf, X. Wang, D.M. Pardoll, J.H. Elisseeff, Design, clinical translation and immunological response of biomaterials in regenerative medicine, Nat. Rev. Mater. 1 (7) (2016) 16040.

[38] L. Cheng, Z. Cai, T. Ye, X. Yu, Z. Chen, Y. Yan, J. Qi, L. Wang, Z. Liu, W. Cui, L. Deng, Injectable polypeptide-protein hydrogels for promoting infected wound healing, Adv. Funct. Mater. 30 (25) (2020), 2001196.

[39] Q. Saiding, J. Jin, M. Qin, Z. Cai, M. Lu, F. Wang, W. Cui, X. Chen, Heat-shrinkable electrospun fibrous tape for restoring structure and function of loose soft tissue, Adv. Funct. Mater. (2020), 2007440.

[40] L. Chung, D.R. Maestas, F. Housseau, J.H. Elisseeff, Key players in the immune response to biomaterial scaffolds for regenerative medicine, Adv. Drug Deliv. Rev. 114 (2017) 184–192.

[41] L. Zhang, Y. Xiang, H. Zhang, L. Cheng, X. Mao, N. An, L. Zhang, J. Zhou, L. Deng, Y. Zhang, X. Sun, H.A. Santos, W. Cui, A biomimetic 3D-self-forming approach for microvascular scaffolds, Adv. Sci. (2020), 1903553.

[42] H. Chen, Y. Cheng, J. Tian, P. Yang, X. Zhang, Y. Chen, Y. Hu, J. Wu, Dissolved oxygen from microalgae-gel patch promotes chronic wound healing in diabetes, Sci. Adv. 6 (20) (2020), eaba4311.